Thin–Walled Structures 157 (2020) 107102

Contents lists available at ScienceDirect

Thin-Walled Structures

journal homepage: http://www.elsevier.com/locate/tws

Full length article

Combined stability of cone-cylinder transition subjected to axial compression and external pressure

M.S. Ismail [a,c], O. Ifayefunmi [b,*], A.H. Mazli [b]

[a] Fakulti Kejuruteraan Mekanikal, Universiti Teknikal Malaysia Melaka, Melaka, Malaysia
[b] Fakulti Teknologi Kejuruteraan Mekanikal dan Pembuatan, Universiti Teknikal Malaysia Melaka, Melaka, Malaysia
[c] Bahagian Kompetensi Dan Peningkatan Kerjaya, Jabatan Pendidikan Politeknik Dan Kolej Komuniti, Putrajaya, 62100, Malaysia

ARTICLE INFO

Keywords:
Cone-cylinder assembly
Buckling
Combined loading
External pressure
Axial compression combined loading
Elastic-plastic
ASME design codes
Equivalent cylinder

ABSTRACT

This paper examines the buckling behaviour of unstiffened mild steel cone-cylinder assembly under (i) axial compression and (ii) combined loading (i.e., axial compression and external pressure). Experimental results on ten (10) laboratory scaled axially compressed cone-cylinder models and their accompanying numerical predictions of collapse load are provided. The tested models are assumed to have the following range of geometric parameter: $r_{cone}/r_{cyl} = 0.565–0.721$, $r_{cyl}/t = 72.17–72.73$, $\beta = 8.536° – 16.69°$ and a constant wall thickness, $t = 1.0$ mm. Result confirms the repeatability of the experimental data. Besides that, there is a good agreement between experimental and numerically predicted collapse load with discrepancy calculated to be within 10%. Furthermore, numerical analysis of stability domains for cone-cylinder assembly subjected to simultaneous load actions of axial compression and external pressure was calculated for a range of geometrical parameters of: (i) $50 < r_{cyl}/t < 400$ and (ii) $10° < \beta < 30°$. For comparison purpose, the equivalent cylinder approach was also deployed to complete calculation based on ASME code case 2286-2. For the case of dimensionless radius-to-thickness ratio, r_{cyl}/t, the result confirms that the ASME code case 2286-2 is unsafe in designing the cone-cylinder shell with $r_{cyl}/t > 400$. Whereas, for the case of different cone angle, β, it can be said that the ASME code case 2286-2 may perhaps be safe to use in designing the cone-cylinder shell with $\beta < 20°$. In addition, the current analysis confirms that increasing the (a) dimensionless radius-to-thickness ratio, r_{cyl}/t and (b) increasing the cone angle, β, may further shrink the combined stability plot. Finally, imperfect cone-cylinder shell under combined loading confirms that (i) the shell is remarkably sensitive at the pressure dominant region compared to the force dominant region and (ii) the location of dimple/dent imperfection at cylinder mid-section proves to be the worst-case scenario.

1. Introduction

Shell combinations such as cylinder with conical end closure are commonly used in many engineering industries. This may be related to aesthetical design and cost reduction factor either in fabrication and operational processes. The joining between two different cylinder diameters can be accomplished by having an insertion of cone section as a transition medium. During service, cone-cylinder transition/intersection shell may be exposed to extreme load in the form of external pressure, axial compression or combination of both. With this kind of load, the main concern must be emphasized towards shells structural integrity, instability and safety. Failure to accommodate the load will result in the structure prone to buckling. Schmidt [1], stated that once a buckle commenced on a cone-cylinder intersection, different treatment is required to handle the structural problem since it is not an individual structural problem (i.e. cone or cylinder). For the case of cone-cylinder shell, the failure mode can be associate with the shape of axisymmetric collapse and predominantly buckle at the junction/joining area. This type of failure may be governed by the effect of shell-discontinuity stresses that intensify the level of compression in the shell (i.e., local buckling) as reported in Zingoni et al. [2,3]. To name a few, the works on the discontinuity shell structure were also reported in Refs. [4–6].

The buckling of axially compressed steel shell assembly (i.e., cylinder-cone-cylinder) interaction was first examined by Knoedel [7]. His work was purely numerical and focused on the elastic buckling of the assemblies under axial compression. Extensive investigation on the

* Corresponding author.
E-mail address: olawale@utem.edu.my (O. Ifayefunmi).

https://doi.org/10.1016/j.tws.2020.107102
Received 20 February 2020; Received in revised form 10 July 2020; Accepted 2 September 2020

buckling of cylinder-cone-cylinder intersection under axial compression using numerical and experimental approaches can be found in Schmidt et al. [8–10]. The membrane theory is also used to support the numerical and experimental results. Eighteen (18) steel shells of different geometrical combination between cone and cylinder were tested. The specimens were made from mild unalloyed steel St12 (Material-No.1.0330). Two different thicknesses were used (0.5 mm and 1 mm) with maximum and minimum diameters set to 450 mm and 159 mm respectively. The numerical analysis was also adopted to support experimental work. The numerical analysis was presented according to the ECCS [11] guideline which consists of (i) linear analysis (LA), (ii) geometrical nonlinear analysis (GNA) and (iii) geometrical material nonlinear analysis (GMNA). From their results, a conservative design approach was recommended which was adopted in ECCS guideline: part C [12].

Schmidt [1,9] reported that a significant difference in buckling mode was identified for the case of axially compressed steel cylinder-cone-cylinder. From the experiment, it was observed that specimen (ZKZ-XV10) experienced a local bending that triggers buckling taking place at a small portion of the large junction area and the cone section. The load-carrying-capacity and the failure mode of cylinder-cone-cylinder transition are reasonably complex under axial load tests. For example, it is argued that the buckling shape switched from the small area junction under linear analysis (LA) to the large area junction via geometrical nonlinear analysis (GNA). Although both analyses are under the bifurcation level [13]. Both numerical analysis (i.e. bifurcation or nonlinear) failed to predict the pattern of buckling mode produced by the specimen. Moreover, for the case of 1 mm thickness, the numerical results (GMNA) underestimated the experiment buckling load. This can be seen for the case of (i) cone-cone combination 14%–26% and (ii) cone-cylinder-cone (i.e. three (3) shells section) to be around 16%–20%. Nonetheless for the case of 0.5 mm thickness, the differences are estimated to be (i) cone-cone combination (14%–19%) and (ii) cone-cylinder-cone (i.e. three (3) shells section) to be around 3%–18%. Knoedel [12] reported that under axial compression, the steel cylinder-cone-cylinder transition with $20^\circ < \beta < 40^\circ$ and $r/t < 200$ failed by axisymmetric buckling (interactive yielding) at the shells junction. The influence of imperfection was reported to be insignificant for this type of failure mode. However, for $r/t > 200$, the shell failed predominated by buckling in the form of non-axisymmetric local yielding at the junction. The influence of imperfection was also examined by adopting the elastic imperfection reduction factor, α for meridional compression as specified in the ECCS [13] recommendation into the perfect shells buckling load (GNMA). The shells buckling loads were later discovered to be conservative. Since the tested specimens experience a minimal geometrical imperfect tolerance, the calculated imperfection is most likely inappropriate. Nonetheless, if the worst-case scenario is considered, then the maximum reduction in load of the imperfect shell is relatively critical [14].

In the early 1970s, tremendous works have been done in investigating the buckling performance of externally pressurize cylindrical shells with conical end closure/segmented shell. Aylward et al. [15,16] presented some experimental and numerical results of nearly perfect steel cone-cylinder intersection. Galletly et al. [17] carried out an experimentally work on six (6) carefully machined cylinder-cone combination subjected to uniform external pressure. The specimens were made from an aluminium alloy (Hiduminium 66 - HE-15) and all the specimens were stress relieved after manufacturing. An accompanying numerical prediction using BOSOR 3 and 5 programs was presented in the paper. The test models were fabricated in the form of identical half-models with different semi-vertex angle ($\alpha = 45^\circ$, 60° and 75°) and length to diameter ratio ($L/D = 0.5$ and 1). The test models were machined from solid billets of aluminium alloy and undergo a quenching heat treatment to minimize the distortion and the formation of residual stresses. Extension of the numerical and experimental works of a similar model was also reported in Ref. [17,18]. Bushnell [19], numerically analyzed Aluminum 2039 cone-cylinder model with similar geometry having a cone angle of 45°. Galletly et al. [17] reported that the obtained experimental and numerical buckling pressures were in a very good agreement (2%–5%). Next, the numerical results from BOSOR 3 showed that all of the tested shells behaved in an axisymmetric mode in the pre-buckling region. The study on combined steel cone and cylinder with various configurations subjected to external pressure were also reported in Ref. [12]. The findings indicated that the numerical results overestimated the experiment. For example, (i) cone-cone combination yielded to be 5%–12% and (ii) combination of three (3) sections (i.e. cylinder-cone-cylinder) amount of 52%–66%. The failure mode was discovered to be a non-axisymmetric buckling for $r/t > 150$. Overall, it may be concluded that the use of cylinder imperfection factor α for external pressure lead to a conservative estimation of buckling pressure.

Shen et al. [20,21] numerically analyzed buckling and post-buckling behaviour of perfect and imperfect unstiffened and stiffened cylindrical shells under combined loading of external pressure and axial compression. Comparative results were made with some available experimental data. It was reported that the buckling and post-buckling behaviour of stiffened and unstiffened cylindrical shells under combined loading primarily depends on three (3) factors: (i) the geometric parameter, (ii) the load proportional parameter and (iii) the imperfection parameter. Ifayefunmi and Blachut [22,23] analyzed the influence of Eigenmode imperfections on the buckling strength of truncated cones subjected to axial compression, lateral pressure, and combined axial compression and external pressure. The cones were assumed to be relatively thick, therefore failing in the elastic-plastic domain. Ifayefunmi [24] adopted ASME case code 2286-2 design procedure to predict the interactive buckling curve of a steel cone. This procedure also suggests a region of safe operational design level for steel cone. The findings from this study show that 'the equivalent cylinders' approach may not represent a safe design for a relatively thick cone under combined loading. To mention a few, experimental investigation on buckling behaviour of reinforced (i.e. stiffened) shells under axial compression were reported in Refs. [25–30] for cone and [31–34] for a cylinder.

To date, there has been little or no information available in the open literature on the stability response of cone-cylinder transition shell subjected to a combined load of axial compression and external pressure. Hence, the current paper provides test data and accompanying numerical results for buckling of cone-cylinder shell subjected to axial compression and further presents a numerical investigation into the combined stability plot for one-cylinder subjected to combined axial compression and external pressure loading.

2. Cone-cylinder - experimentation

2.1. The fabrication process, pre-test and material properties

Ten (10) laboratory scaled cone-cylinder transition shells were fabricated using 1 mm mild steel sheet. As illustrated in Fig. 1 (a), the specimens were assumed to have nominal geometry given by: $r_{cone}/r_{cyl} = 0.565–0.721$, $r_{cyl}/t = 72.17–72.73$, $\beta = 8.536^\circ - 16.69^\circ$ and wall thickness, $t = 1.0$ mm. Whilst the cone axial length and the cylinder axial length was varied between 100 mm – 200 mm, respectively. It is worth mentioning that the abbreviation 'F' and 'P' specifically indicate the type of loading condition prior to buckling. All shells were assumed to have a constant nominal radius for cylinder, $r_{cyl} = 70$ mm and two (2) different nominal radii for cone, $r_{cone} = 40$ mm and 50 mm. To ensure repeatability of experimental data, each of the specimens was identically manufactured in pairs. This would provide two experimental data values for a cone-cylinder with nominally the same dimension. Specimens were designated as (e.g. CC1-AC). The 'CC' is denoted as cone-cylinder, while the following number indicates the number of specimens. Additionally, the abbreviation 'a' and 'AC' designated as identical shell geometry and type of load (e.g., axial compression). For example, CC2a-AC denotes cone-cylinder shell number 2 (e.g. cone-cylinder transition) subjected to

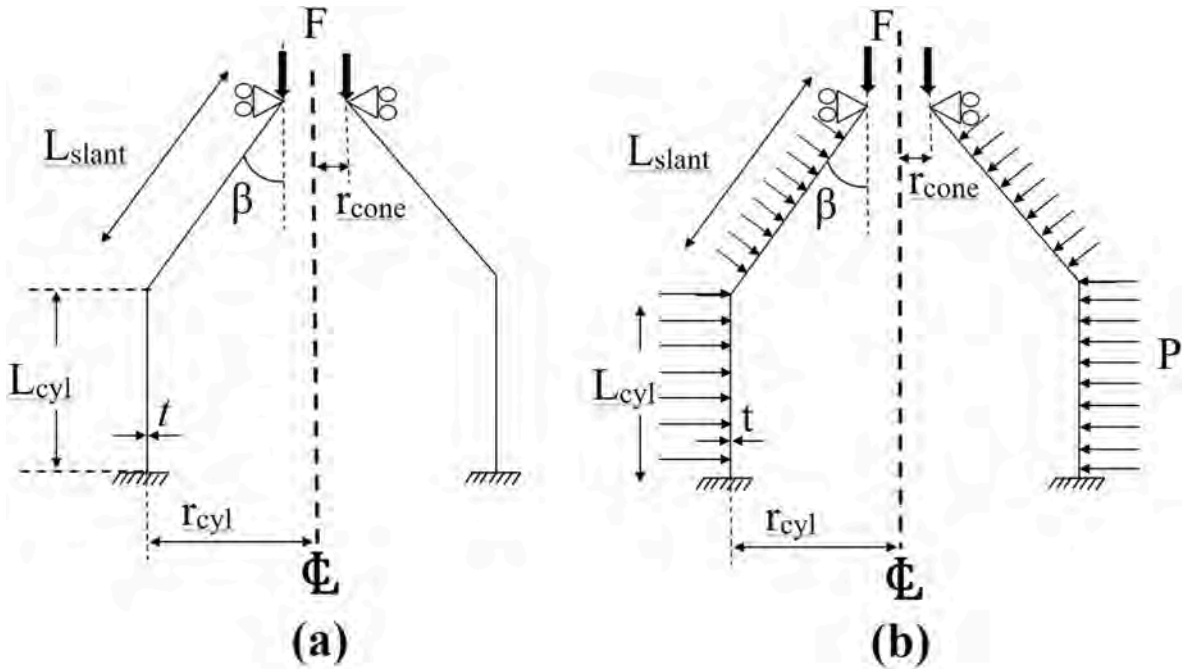

Fig. 1. (a) Geometry and boundary condition of cone-cylinder shell subjected to axial compression and (b) combined between axial compression and external pressure. N.B: 'F' = axial compression and 'P' = external pressure.

axial compression. This specimen is somewhat identical to CC3a-AC model.

First, the tensile test was conducted separately to extract the material properties of mild steel. Six (6) coupon specimens were cut from steel sheet for tensile test. The samples were designed according to British Standard [35]. Three (3) coupon specimens were cut in the vertical direction while another three (3) were cut in a horizontal direction of the steel sheet. The coupon specimens have not undergone any heat treatment. Full engineering stress-strain were extracted from the tensile test. Overall, the results of the tensile test are given in Table 1. It can be seen that the average value of Young's Modulus was found to be 193.667 GPa. Conversely, the obtained yield stress was 216.96 MPa. To note, the mild steel material yield point was based on 0.2% of proof stress. The average value of Young's Modulus, E, and yield stress, $\sigma_{yield\ upper}$ were used in the numerical analysis. Fig. 2 illustrates a plot of stress-strain tensile test exemplified by H1 specimen.

Next, specimens were cut from 1 mm mild steel plate using waterjet machining. After the cutting process, the samples were rolled into the conical and cylindrical form using a conventional rolling machine. Then, Metal inert gas welding (MIG) was used to weld the seam between the two neighbouring longitudinal free edges of the cones and cylinders, separately. Afterwards, the circumferential ends of both cone and cylinder were welded together using the same welding process.

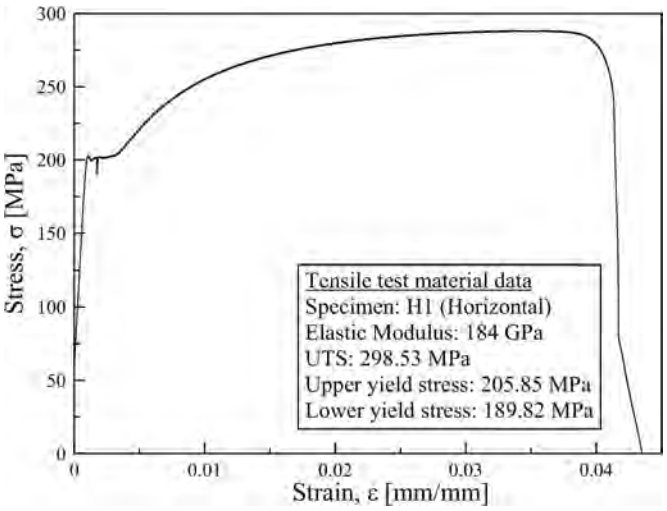

Fig. 2. Plot of stress-strain tensile test exemplified by H1 specimen.

Table 1
Set of material data obtained from uni-axial tensile tests on mild steel plate (E = Young's modulus, σ_{yield} = yield stress, and UTS = ultimate tensile strength). Note: The upper and lower yield value were taken from 0.2% of proof stress.

Sample	Orientation	E	$\sigma_{yield\ upper}$	$\sigma_{yield\ lower}$	UTS
		[MPa]			
1	H1	183905.69	205.85	189.82	298.53
2	H2	175158.97	215.89	200.85	307.56
3	H3	145354.12	230.48	216.62	322.11
4	V1	202851.73	214.86	203.73	305.69
5	V2	201402.04	222.66	216.99	305.68
6	V3	157872.88	218.06	213.03	303.32
Average (H1-H3)		168139.59	217.41	202.43	309.4
Average (V1-V3)		187375.55	218.53	211.25	304.9
Average (All)		193667.1667	217.97	206.84	307.15

3. Collapse test and results

Before the buckling test, some measurement was taken on all the cone-cylinder specimens. First, the wall thickness was measured using micrometre screw gage at a different equidistant point along each meridian. This was then repeated 36° spaced across the circumference. Table 2 presents the nominal, minimum, maximum and average measured thickness. The average measured geometry of cone-cylinder shells (mid-surface values where appropriate) that consist of the cone height, cone slant length and cylinder height are given in Table 3. Fig. 3 plotted the scatter of measured wall thickness along the height for all tested cone-cylindrical specimens.

Cone-cylinder shells (CC1-AC, CC2a-AC, CC3a-AC, CC4-AC, CC5-AC, CC6-AC, CC7-AC, CC8-AC, CC9-AC and CC10-AC) were tested using 100

Table 2
Measured data of the wall thickness for all tested cone-cylinder specimens.

Models	t_{nom} (mm)	t_{min}	t_{max}	t_{ave}	t_{std}
CC1-AC	1.0	0.94	0.965	0.9508	0.008924
CC2a-AC	1.0	0.94	0.965	0.9513	0.008222
CC3a-AC	1.0	0.935	0.965	0.9515	0.007942
CC4-AC	1.0	0.94	0.965	0.9509	0.008311
CC5-AC	1.0	0.94	0.965	0.9526	0.006913
CC6b-AC	1.0	0.94	0.965	0.9499	0.009032
CC7b-AC	1.0	0.94	0.965	0.9532	0.00584
CC8-AC	1.0	0.94	0.965	0.9501	0.008761
CC9-AC	1.0	0.94	0.965	0.9507	0.008676
CC10-AC	1.0	0.94	0.965	0.9502	0.008666

Table 3
Average measured geometry of cone-cylinder shells (mid-surface values where appropriate).

Model	[mm]				β (°)
	r_{cone}	r_{cyl}	L_{cyl}	L_{slant}	
CC1-AC	49.856	69.188	100.031	101.988	11.348
CC2a-AC	39.081	69.136	99.990	104.419	16.689
CC3a-AC	39.878	69.158	100.018	104.417	16.667
CC4-AC	39.746	68.788	100.002	202.258	8.536
CC5-AC	39.684	69.153	99.978	152.989	18.417
CC6b-AC	39.521	68.719	100.013	152.989	11.337
CC7b-AC	39.401	68.992	99.983	94.905	11.323
CC8-AC	39.36	69.31	100.48	104.32	17.60
CC9-AC	39.31	69.24	149.71	104.82	17.00
CC10-AC	39.28	69.20	196.95	104.47	16.90

Fig. 4. Test set-up for cone-cylinder specimen under axial compression only.

kN Shimadzu compression machine. Before testing, the specimens were covered with top and bottom plates as depicted in Fig. 4. This is presumed to create the necessary boundary condition for the experiment i.e., fixed condition at the bottom (i.e., $u_x = u_y = u_z = \phi_x = \phi_y = \phi_z = 0$) and only allow axial movement at the top while all other are constrained

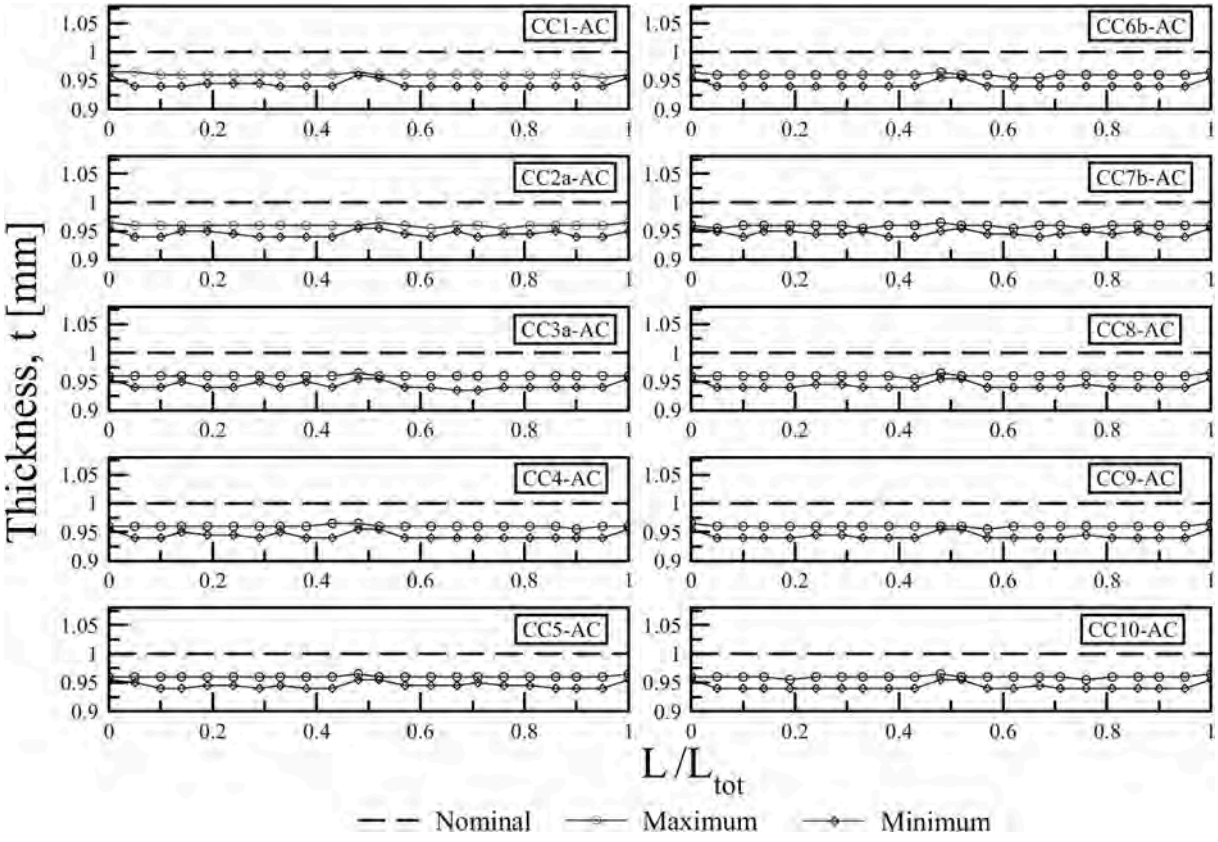

Fig. 3. Scatter of measured wall thickness along the height for all tested cone-cylindrical specimens.

(i.e., $u_x = u_z = \phi_x = \phi_y = \phi_z = 0$, and $u_y \neq 0$). It is assumed that the platen of the Shimadzu machine will help to provide the desired boundary condition. However, it is worth mentioning here, that the plate and specimen was assumed to be tight-fitted with no rotation during the experiments. Though it is practically impossible to achieve fully clamped condition without rotation, the effect of rotation on the magnitude of the buckling load of a cylindrical shell has been proven to be marginal [36]. Incremental axial load was applied to the upper end of the cone-cylinder at the rate of 1 mm/min. This is the same rate of loading used to obtain the material properties of the mild steel plate from which the cone-cylinder specimens were made. The incremental axial load was applied to the cone-cylinder shell until the specimen fails. The compression extension and the corresponding load at each increment were recorded by the machine. To verify the deformation recorded by the machine controller, it was decided to use two clock gauges positioned on the top covering plate of the small end of the cone (see Fig. 4). This was done to measure the actual shortening of the cone-cylinder shell during the experiment. However, the gauges were not connected to any online system, the reading was taken manually. Hence, only one gauge was recorded up to the collapse load. And the corresponding load at instant compression extension were directly taken from the load indicator on the machine.

Fig. 5 presents the plot of experimental load against axial shortening for cone-cylinder CC2a-AC. From Fig. 5, it is apparent that readings given by the clock gauge produce a plot that has a similar trend to that of the machine controller. Also, the plot from the clock gauge produces a marginal stiffer slope as compared to the plot from the machine controller. This can be attributed to the contribution of the measurement of deformation from the crosshead movement. Fig. 6 presents the magnitude of the collapse load for all tested cone-cylinder models. This results explicitly shows that the shell's geometry such as (i) radius (i.e., cone and/or cylinder), (ii) length (i.e., cone's slant and/or cylinder) and, (iii) semi vertex angle, play a significant role in influencing the load-carrying capacity of the cone-cylinder specimen. For example, model CC1-AC demonstrates that when the radius of cone increases, it costs a decrease of buckling load. Then again, model CC4-AC exhibit the smallest cone angle with highest slant length thus produces a second largest magnitude of buckling load. Models CC5-AC, CC6b-AC and CC7b-AC on contrary exhibit the lowest magnitudes of buckling load. Subsequently, model CC5-AC represent the largest cone angle of 18.417°, thereby as expected, produces one of the lowest buckling load. This finding is somewhat similar to what been reported in Ref. [27]. Again, from Fig. 6, it is apparent that two identical specimens with the same loading condition (i.e., CC2a-AC, CC3a-AC, CC6b-AC and CC7b-AC) yield a close experimental collapse load within 1.5%–5% of differences. Hence, confirming the repeatability of the experimental data.

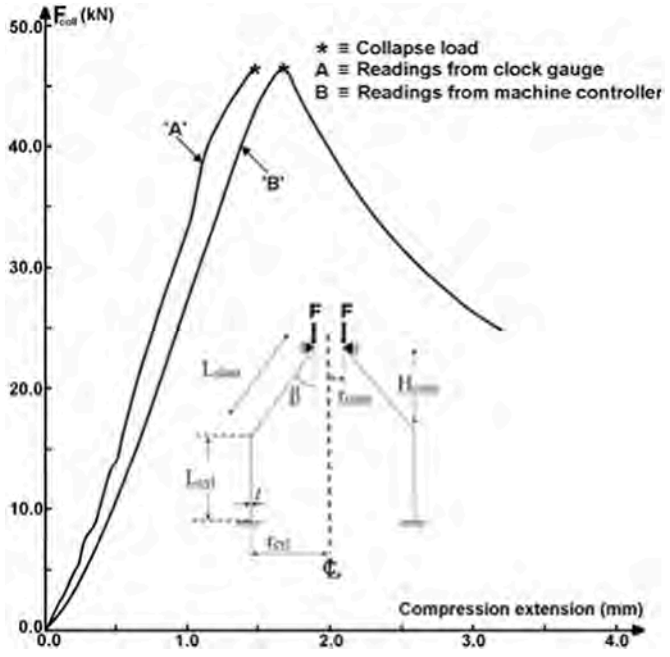

Fig. 5. Plot of load versus compression extension for cone-cylinder specimen CC2a-AC subjected to axial compression only.

Fig. 7 depicts the photograph of selected specimens after being tested. It can be seen that the tested models failed in an axisymmetric pattern, with junction/transition area being mostly severed. While the conical and cylinder part remained in membrane state, the failure mostly occurred in the form of bending at the junction due to concentrated discontinuity stresses. As expected, this can be attributed to membrane stress discontinuity at the intersection, reflecting the localized and rapidly changing behaviour of bending disturbance. That is, under various loading conditions, the state of stress in the multi-segment shell of revolution assembly (cone-cylinder assembly) is predominantly membrane stress away from the intersection, but as the intersection is being approached from either the top or the bottom, the state of stress in the shell will change from membrane stress to a combination of membrane stress and bending stress [2].

4. Cone-cylinder numerical modelling

Consider a cone-cylinder transition shell with small and big radii r_{cone} and r_{cyl} respectively, uniform wall thickness, t, slant length of the cone, L_{slant}, length of the cylinder, L_{cyl} and cone angle, β, as depicted in Fig. 1. Different cone angles were considered, with the range of $\beta = 8.5^{\circ} - 18.4^{\circ}$. The cone-cylinder transition is subjected to axial compression (Fig. 1 (a)) and the simultaneous action of axial compression and external pressure (Fig. 1 (b)). It is assumed that the cone-cylinder transition is fully clamped at the bottom end (i.e., $u_x = u_y = u_z = \phi_x = \phi_y = \phi_z = 0$), and the other end (i.e., the top end of the cone) is only allowed to move in the axial direction (i.e., $u_x = u_z = \phi_x = \phi_y = \phi_z = 0$, and $u_y \neq 0$). The shell is made from mild steel with the following material data obtained from the experiment (see section 2.1 for more detail): Young's Modulus, E = 193.667 GPa and Yield's stress, σ_{yp} = 217.97 MPa. Poisson's ratio, ν, of the mild steel was assumed to be 0.3 (taken from the material datasheet). The material is modelled as elastic perfectly-plastic. Nonlinear static Riks analysis was employed in the numerical analysis. In the finite element calculations, J2 flow plasticity theory was adopted. The finite element (FE) analysis was carried out using the four-node shell element with six degrees of freedom (S4R in ABAQUS element library). Since the shell is a joining assembly between cone and cylinder, it should be treated differently in terms of buckling analysis unlike the single shell (e.g., cone and cylinder), as it may possess the discontinuity stress effect. The equation of continuity of displacement at the cone-cylinder intersection is given by: $u_{x(cyl)} = \bar{u}_{x(con)}$; $u_{y(cyl)} = \bar{u}_{y(con)}$ and $u_{z(cyl)} = u_{z(con)}$. The notation used above assumes u ≡ displacements (u_x, u_y, u_z are local coordinate and $\bar{u}_x$, $\bar{u}_y$, $\bar{u}_z$ are global coordinate).

Numerical calculations were carried out using ABAQUS FE software to (i) serve as a benchmark for the experimental data, and (ii) provide further analysis for cone-cylinder shells with varying geometric parameter under different loading condition. This seems necessary to confirm the appropriateness of the numerical approach adopted in this paper. It is customary in numerical analysis to test the mesh sensitivity of the FE model based on their accuracy. Table 4 shows that 2960 elements are sufficient for the numerical analysis by taking CC2a-AC model as an example.

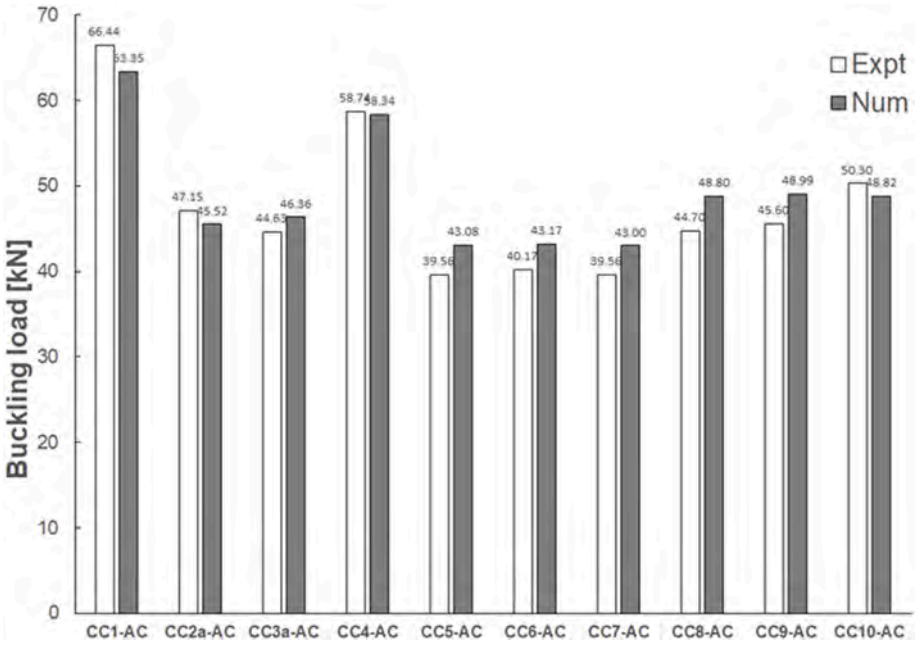

Fig. 6. Comparison of numerically obtained buckling load with experimental results for cone-cylinder models.

Fig. 7. Photograph of selected cone-cylinders specimens after testing.

Table 4
Numerical result on mesh sensitivity demonstrate by CC2a-AC model.

Mesh size	740	1170	2960	4743	8308
Collapse load, F [kN]	40.221	42.788	45.519	46.429	46.890

5. Numerical results

5.1. Comparison of experimental and numerical results for cone-cylinder subjected to axial compression

Fig. 6 depicts the comparison of experimental collapse load against numerical predictions for all tested cone-cylinder shells together with their corresponding magnitude of collapse loads. From the results, it is apparent that the collapse loads numerically calculated by the FE model are in a good agreement with experiment. The percentage difference was calculated to range from +5% to −8% in comparison with the experimental data. The highest percentage of differences in a comparison between experimental and numerical were recorded for CC5-AC, CC7b-AC and CC8-AC models. On the other hand, CC4a-AC model revealed to be the closet ones, with about 1% of a discrepancy. To enclose, it is appropriate to highlight a good agreement demonstrated by our numerical model with the obtained tested data as the overall discrepancy was calculated to be within 10%. Thereby, confirm the appropriateness of the numerical approach adopted in this paper.

In the FE analyses, average geometry has been used by incorporating measured shape and variable wall thickness. It is noted here that all experimental ratio values are between 0.916 and 1.049 (i.e., lower and higher) to the numerical predictions. Most likely, this may be associated with: (i) strain hardening of steel, (ii) variation of wall thickness nearby the weld join region and (iii) existence of shape imperfections that might occur during the fabrication process.

5.2. Numerical predictions for cone-cylinder shell subjected to axial compression or external pressure only

The plot of collapse or bifurcation load for cone-cylinder shell subjected to axial compression and external pressure individually, are shown in Fig. 8 (a) - (d). In this section, a collapse/bifurcation analyses of the cone-cylinder shell with variation of (i) radius-to-thickness ratio, r_{cyl}/t and (ii) cone angle, β are presented. The first set of results was obtained for the case of an axially compressed cone-cylinder shell as shown in Fig. 8 (a) - (b). To execute the analysis, the top and bottom radius of a cone were kept constant, as the angle of the cone, β, is then varied between $10^{\circ}<\beta<30^{\circ}$. This dimensional adjustment may result in a change of cone slant height, L_{slant} as the cone angle, β. From the analyses, it is evident that there is a substantial decrease of the collapse load with a greater value of (i) r_{cyl}/t and (ii) angle of the cone, β as shown in Fig. 8 (a)–(b). For the case of different radius-to-thickness ratio, r_{cyl}/t, a steady drop of collapse load is observed, as the results also indicated that the shell with $r_{cyl}/t = 400$ is mostly 92% weaker than the $r_{cyl}/t = 50$ shell. A sharp drop of collapse load is also observed for the case of cone angle between $10^{\circ}<\beta<30^{\circ}$, with 44% decreases of load-carrying-capacity calculated. The plotted results are identical to what has been reported in Ref. [37].

Fig. 8 (c) - (d) illustrate the results of cone-cylinder shell under external pressure for different (i) r_{cyl}/t and (ii) cone angle, β. It is worth to mention that the set of results are represented in the form of collapse and bifurcation. For the case of different radius-to-thickness ratio, r_{cyl}/t, a steady drop of collapse load is also observed for this case with the drop of load-carrying capacity was recorded to be nearly 97%. Surprisingly, the drop in shell load-carrying capacity is nearly identical in comparison to the case of a shell with an axial compression load. Nonetheless, for cone-cylinder with different cone angle, β, a slight increase of collapse load is seen at the small cone angle, after which the plot remains linear. In general, the given results confirm that externally pressurized cone-

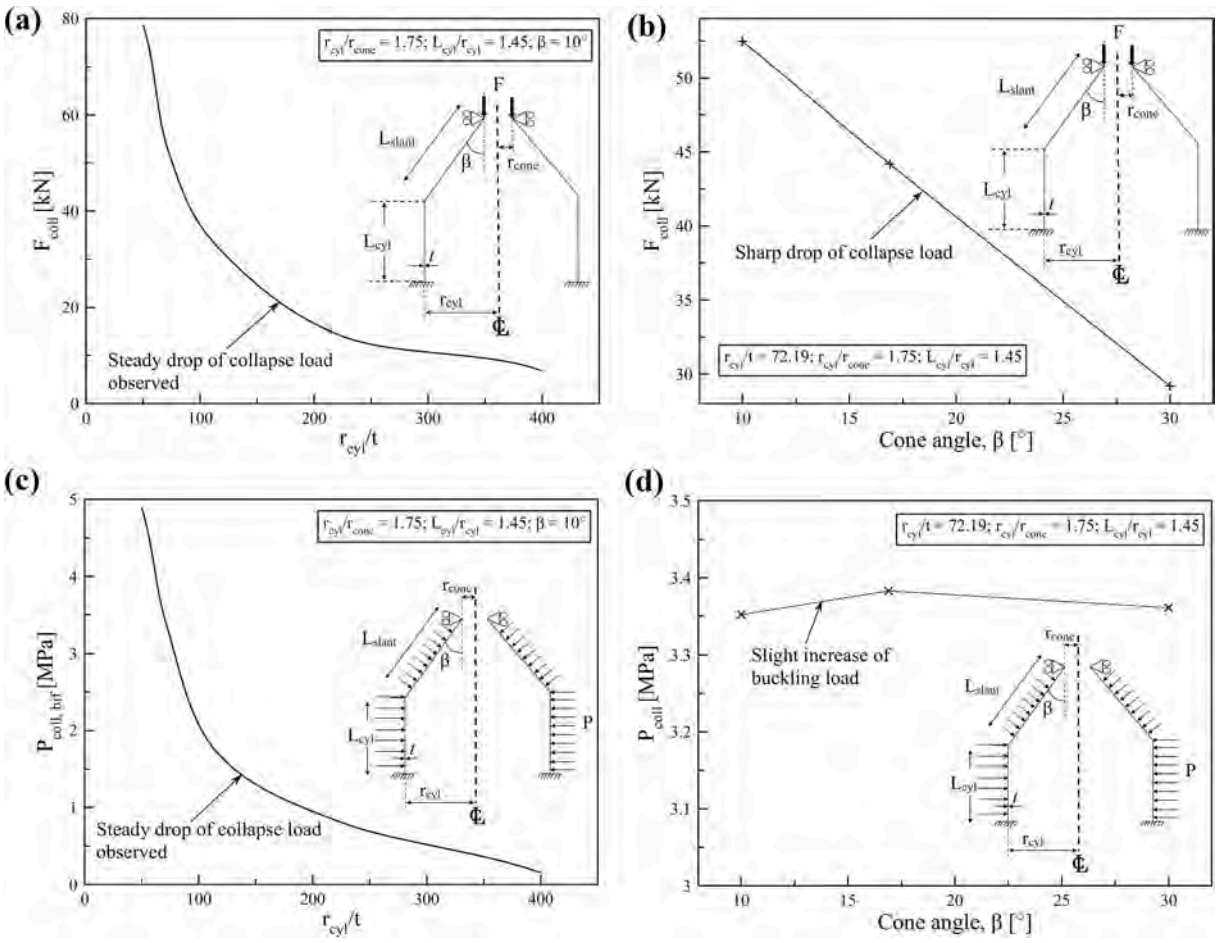

Fig. 8. Plot of collapse load of cone-cylinder shell subjected to axial compression against (a) dimensionless-radius-to-thickness ratio and (b) cone angle. The plot of collapse/bifurcation load of cone-cylinder shell subjected to external pressure against (c) dimensionless-radius-to-thickness ratio and (d) cone angle.

cylinder shell with different radius-to-thickness ratio, r_{cyl}/t contribute the biggest factor in influencing the shell's strength.

5.3. Numerical predictions for cone-cylinder shell subjected to combined axial compression and external pressure

This section aims to analyse (i) the shape of combined stability plot/domain and, (ii) check the applicability of existing design guideline/code on combine stability by prescribing ASME case code 2286-2 as a comparative case. However, since there is no available design code for the cone-cylinder shell under combine loading (i.e., axial compression and external pressure) thus a cone with the identical dimension with cone-cylinder shell were taken as a benchmark model and analyzed based on ASME code case 2286-2 [38]. The numerical results were calculated using ABAQUS FE code for cone-cylinder shells with geometrics characteristics by (i) $50 < r_{cyl}/t < 400$ and (ii) $10^\circ < \beta < 30^\circ$. During numerical calculation, two (2) types of analysis were performed, they are; (i) bifurcation buckling analysis and (ii) collapse (static Riks) analysis. The shell's yield envelope was obtained using ABAQUS FE Code. Asymmetric bifurcation and axisymmetric collapse loads of cone-cylinder shells were calculated using ABAQUS FE Code. Asymmetric bifurcation buckling loads were calculated using ABAQUS eigenvalue buckling procedure based on subspace solver. For the case of asymmetric bifurcation analysis, the steps involve by prescribed a non-linear static general step first, to induce a preloaded step and followed by a buckle step. The lowest computed eigenmode of interest is taken to be the bifurcation buckling load of cone-cylinder shell. The collapse load, on the other hand, was numerically calculated using the Riks method.

There are several steps required to accomplish the interactive curve. They are listed below for the case of collapse:

a) Calculate the collapse force, Fcoll under pure axial compression;
b) Calculate the collapse pressure, Pcoll under pure external pressure;
c) Calculate the collapse load subjected to combined loading, (i.e., axial compression and external pressure acting simultaneously using a combination of loading path; and
d) Calculate the first yield load for the cone-cylinder shell for the case of (i) pure axial compression, (ii) pure external pressure and, (iii) combined loading.

Buckling analysis of cone-cylinder shell subjected to combine load action of external pressure, P and axial compression, F that acts simultaneously depends on the relative magnitude of, P, and F applied on the structures. It is customary to represent the buckling strength of cone-cylinder shells through interactive diagrams (i.e., combined stability plot). Taking cone-cylinder shell of $r_{cyl}/r_{cone} = 1.75$, $r_{cyl}/t = 72.19$, and $\beta = 16.89^\circ$ as example, a typical combined stability plot is shown in Fig. 9. In detail, two (2) distinct regions can be identified in Fig. 9, they are; (i) 'X' – force dominant region, where the collapse/failure of the cone-cylinder shell is governed by axial force and (ii) 'Y' – pressure dominant region, where the failure of the shell is controlled by external pressure. This means that in each region either 'X' or 'Y' constant load of known magnitude (i.e., axial compression or external pressure) is applied to determine the other counterpart magnitude of load that will cause failure. The interactive stability curve often represents by two (2)

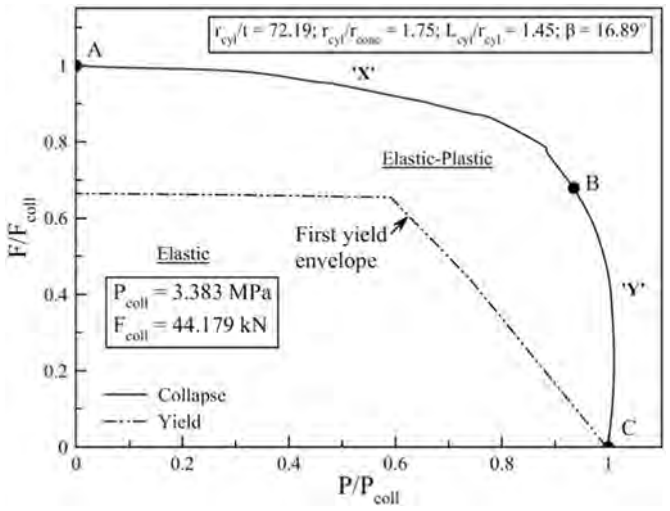

Fig. 9. Typical combined stability plot for cone-cylinder transition of $r_{cyl}/r_{cone} = 1.75$, $r_{cyl}/t = 72.19$, and $\beta = 16.89°$.

distinct domains, they are (i) elastic and (ii) elastic-plastic. This has been represented by the continuous and dotted lines which denotes a collapse and yield loads, respectively. By means, it indicates that the region below dotted line (i.e., first yield envelope) is considered to be elastic and the area beyond the dotted line is elastic-plastic. Fig. 10 (a) - (c) plotted the load versus deflection of the cone-cylinder shell under (a) axially compressed, (b) externally pressurized and, (c) combined of both loads. Moreover, Fig. 10 (b)–(c) denotes a collapse load of external pressure against the shell's deflection. Expectedly, it been noted that the collapse load produced by external pressure is greater than the combined loading with a disparity amount of 6.5%. This situation is explained, as the combination of both loads (i.e., axial compression and external pressure) that act together, severely weaken the shell further. Again, the load-deflection curve is linear up to the collapse load is reached, once the collapse load is reached, it followed by a stable drop as observed for the shell subjected to (i) axial compression and (ii) combined loading. The shell under external pressure does not experience any significant drop of buckling load once the collapse load is reached. Surprisingly, a different behaviour was observed from Fig. 10 (c) for combined axial compression and external pressure, as the initial/starting point of the load was slightly offset (i.e., $\delta = 0.125$ mm). Again, this can be described as the combination load was executed based on sequential period; primarily, the shell was axially compressed with a constant load of $F_{const} = 30$ kN and followed by external pressure until it reached collapse. Thereby, under axial compression, the cone-cylinder structures experience an axial shortening in the length as a result of axial compression of the structure. Once it experiences an axial shortening, the shell further shrinks due to the excessive amount of deformation from the external pressure load.

Fig. 11 presents the plots of a dimensionless ratio of plastic deformation-over-thickness (i.e., w/t) of a cone-cylinder shell at peak/collapse load subjected to (i) axial compression, (ii) external pressure and, (iii) combination of both. The point of interest in this analysis lies in the deformation/plasticity of the shell through collapse mode. The

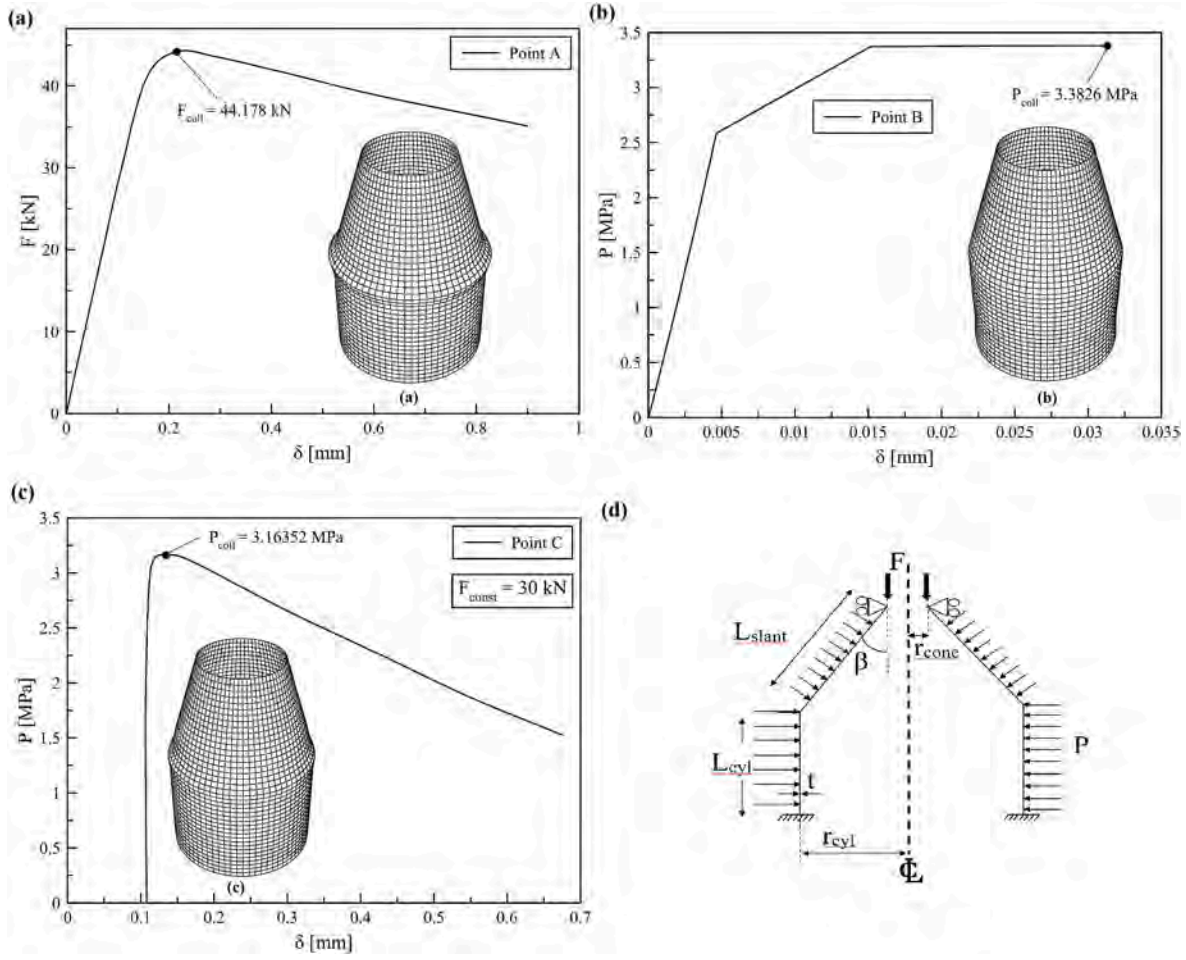

Fig. 10. Plot of load versus deflection of cone-cylinder shell subjected to (a) axially compressed, (b) externally pressurized and, (c) combined of both loads. The boundary condition of the shell under (d) combined loading.

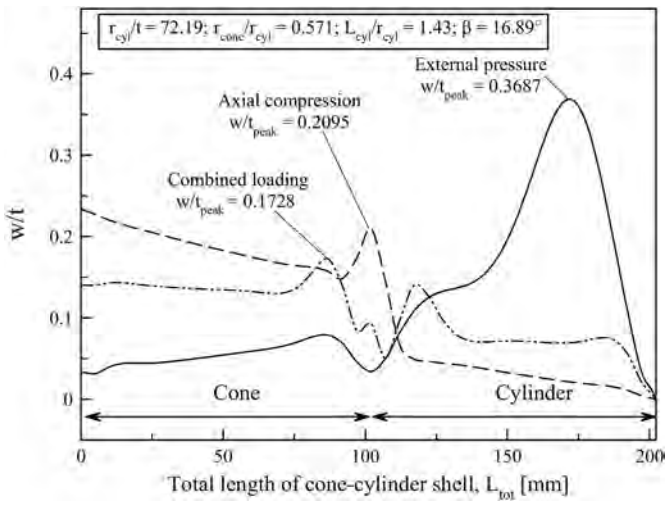

Fig. 11. Dimensionless ratio of plastic deformation-over-thickness (i.e., w/t) of a cone-cylinder shell at peak/collapse load subjected to (i) axial compression, (ii) external pressure and, (iii) combination of both.

points of interest were taken along the meridional line (e.g., total shell length) of the cone-cylinder structure. The starting point was taken at the cone top node and end-up at the bottom node of the cylinder. Then again, a total of 40 nodes were selected for the analysis. Several points can be drawn from the given result. As expected, the shells failed predominantly at the intersection area (i.e., between the bottom of the cone and top of the cylinder) under axial compression and combined loading. Besides failure at intersection area, the shell also seems to be slightly unstable at the conical section, under axial compression. On the contrary, for cone-cylinder subjected to external pressure, the shell failure was more prominent in the cylinder region. The externally pressurized shell was seen to experience the largest plastic deformation with a magnitude of $w/t_{peak} = 0.3687$, followed by shell subjected to axially compressed and combined loadings with the magnitude of deformations recorded to be $w/t_{peak} = 0.2095$ and $w/t_{peak} = 0.1728$, respectively. Unsurprisingly, the shell failed at the junction for both conditions (i.e., (i) axial compression and (ii) combined loading). This behaviour may attribute to the discontinuity slope in the shell meridian at the junction, thereby ensuing in local bending and circumferential stresses at the intersection [2]. Also, under these types of loading conditions (e.g., (i) axial compression, (ii) external pressure and, (iii) combination of both),

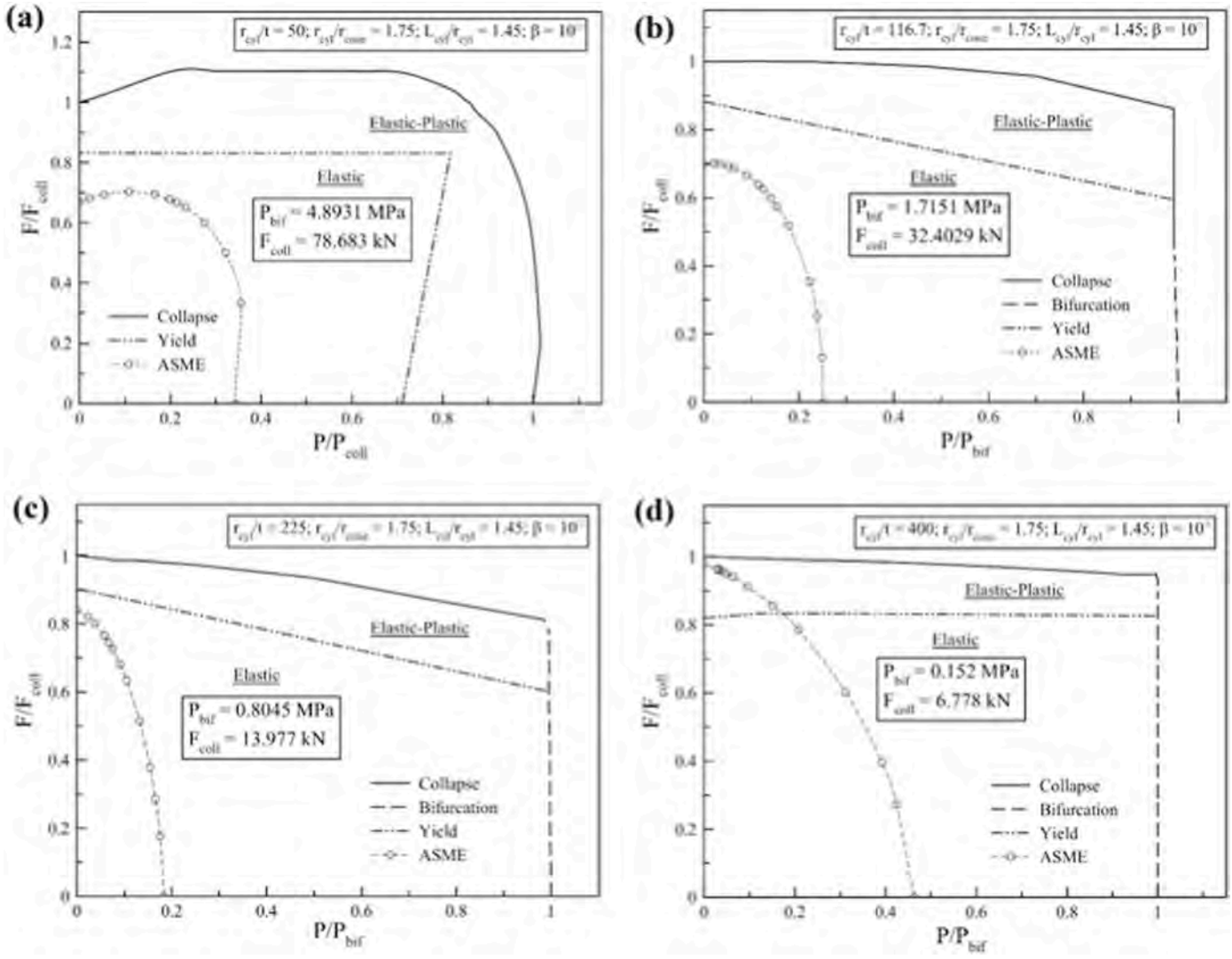

Fig. 12. Combined stability plot for cone-cylinder transition shell in the range of $50 < r_{cy}l/t < 400$ with constant $\beta = 10°$.

the state of stress in multi-segment shell assembly is pre-dominantly membrane stress that locates away from the intersection, however, once the intersection being approached from either top or bottom of the shell, it will result to a sudden change from membrane stress to a combination of membrane and bending stresses as reported in Ismail et al. [39]. Alternatively, some study may recommend strengthening the cone-cylinder shell structure by introducing a reinforcement or either increasing the thickness of the shell at the junction [1,3,40]. From the analysis, it can be concluded that the characteristic of deformation and plasticity of a cone-cylinder shell (i.e., buckled at the intersection) is most likely similar to what been reported in (i) cylinder-cone-cylinder shell [12,39] and (ii) torispherical shell [41,42], as those mentioned structures are associated with multi-segmented shell assembly.

Fig. 12 (a) – (d) presents the numerical predictions for comparisons of combined stability plot for the cone-cylinder shell with the range of the dimensionless radius-to-thickness ratio of 50 $<r_{cyl}/t<$ 400 subjected to combined loading of axial compression and external pressure. Furthermore, an analytical calculation based on ASME code case 2286-2 [38] was also included in the analysis for comparison purpose. This approach is essential from the practical point of view in designing the shell structure under combined loading, (i.e., axial compression and external pressure). The equivalent cylinder approach was also deployed to complete calculation based on ASME code case 2286-2 for a comparison purpose. It is worth noting that for each analyzed shells, 25 different points data via numerical calculation are required to complete the interactive plot. From Fig. 12 (a)–(d), it is explicitly evident that the entire combined stability plot displays a similar trend, except for $r_{cyl}/t <$ 116.7, where the load-carrying capacity of the cone-cylinder shell is always governed by axisymmetric collapse. On the other hand, for the case of $r_{cyl}/t >$ 116.7, the failure of the tested shell is controlled by two (2) mechanisms of failure, i.e., (i) asymmetric bifurcation and (ii) axisymmetric collapse. It may be seen that once the axial load approaches the collapse magnitude, the resistance of external pressure progressively diminished. Moreover, the mode of failure is also changed from asymmetric bifurcation to axisymmetric collapse. Interestingly, the plotted interactive curve of ASME code case 2286-2 illustrates that increasing the range of dimensionless radius-to-thickness ratio may significantly affect the collapse load governed by axial force. In contrast, the design code slightly affects the shell's failure that has been governed by external pressure. Both of these conditions are demonstrated for the case of the large shell (i.e., $r_{cyl}/t =$ 400). Furthermore, the interactive stability plot estimated by ASME code case 2286-2 slightly exceeds the elastic-plastic domain at the 'force dominant region' for the case of a cone-cylinder shell of $r_{cyl}/t =$ 400. The result thereby confirming the unsafeness of ASME code case 2286-2 in designing the cone-cylinder shell with $r_{cyl}/t >$ 400. Fig. 13 confirms that increasing the range of dimensionless radius-to-thickness ratio will shrink the combined stability plot.

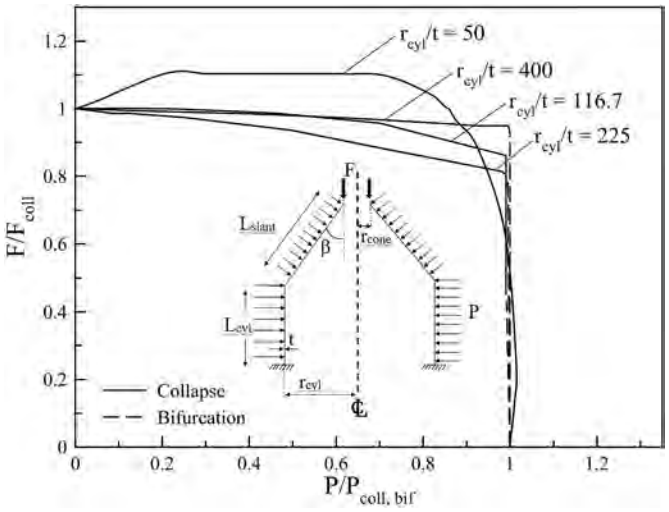

Fig. 13. Domain of combined stability plot for different r_{cyl}/t values.

Fig. 14 (a) – (c) shows the plot of interactive combined stability of cone-cylinder shells with a different cone angle of 10°$<\beta<$ 30°. From the combined stability plot, it can be seen that there is no effect of asymmetric bifurcation experience by the cone-cylinder shells by changing the cone angle. Since there is no study involving stability plot of cone-cylinder under combined load action, it may be noted here that changing the angle of the cone possibly will lead to (i) consistent/identical shape of the typical combined interactive plot and (ii) shrinking the interactive plot for a shell with large cone angle. Again, the design recommendation by ASME code case 2286-2 was employed as a comparative purpose. It indicates that the interactive stability plot estimated by ASME code case 2286-2 surpassing the elastic-plastic region with the increment of cone angle, $\beta >$ 20° (see Fig. 14 (b)–(c)). Fig. 14 (c) shows an overestimation beyond the collapse line was predicted by the design code for the case of a cone-cylinder shell with a cone angle of, $\beta =$ 30°. The following cases of overestimation of collapse load took place at the 'force dominant region'. This issue could be associated with the equivalent cylinder approach, as it might transform the shell to be extensively larger, hence increasing the estimation of the load-carrying capacity. This rather more likely to be prominent for the case of the axially compressed cone-cylinder shell. Eventually, it can be said that the ASME code case 2286-2 may perhaps be safe to use in designing the cone-cylinder shell with $\beta <$ 20°, and constant $r_{cyl}/t =$ 72.19 and $r_{cyl}/r_{cone} =$ 1.75. Fig. 15 point out a reduction of the combined stability plot by increasing the cone angle. In general, It is worth to remark that the current result supports the finding reported in Ref. [24].

Fig. 16 (a) – (b) depict the plot of the area of plastic strains within combined stability domain to the total area, A_{pl}/A_{tot}, against range (i) dimensionless-radius-to-thickness ratio, 50 $<r_{cyl}/t<$ 400 and (ii) cone angle, 10°$<\beta<$ 30°. A recorded progressive growth of plastic deformation is seen for the case of $r_{cyl}/t <$ 100 as shown in Fig. 16 (a). Additionally, the cone-cylinder shell of, $r_{cyl}/t =$ 50 indicates about 50% of shell wall undergoes a plastic straining. A stable drop of plastic strain is also observed for the range of shell with a dimensionless-radius-to-thickness ratio of, 200$<r_{cyl}/t <$ 400. Next, Fig. 16 (b) plots a plastic strain domain against cone angle, β for a cone-cylinder shell with a range of 10°$<\beta<$ 30°. From the plotted data, a different curve characteristic was observed in comparison to the shell with different r_{cyl}/t. An obvious climb of plastic strain (i.e., A_{pl}/A_{tot}) is seen for the range of cone angle, $\beta <$ 20°. The plotted curve is then reached a little plateau before undergoes another slight climb at $\beta =$ 20°. Nonetheless, the differences of plastic strain are recorded to be about 18%. In contrast, the calculated differences are not fairly apparent for the case of different range of cone angle, compared to the shell with different r_{cyl}/t. From the given results, it can be underlined here that the cone-cylinder is relatively sensitive to the plastic strain at the wall thickness for the case of different r_{cyl}/t in comparison to the changes in cone semi-vertex angle, β. This situation may be linked with the design of the cone-cylinder itself, for example, by having a thinner shell could be resulting in a significant reduction of shell wall, thereby consequent a magnitude of sensitivity in term of plasticity.

5.4. Numerical predictions for imperfect cone-cylinder shell subjected to combined axial compression and external pressure

In this section, the imperfect cone-cylinder shell subjected to combined axial compression and external pressure was numerically analyzed by employing the Single Load Indentation (SLI) imperfection technique via static Riks analysis. The SLI imperfection approach was considered to be the worst and realistic imperfection technique when considering the imperfection sensitivity of shell structures [43]. This concept is explained by creating a local inward dent from indentation(s)

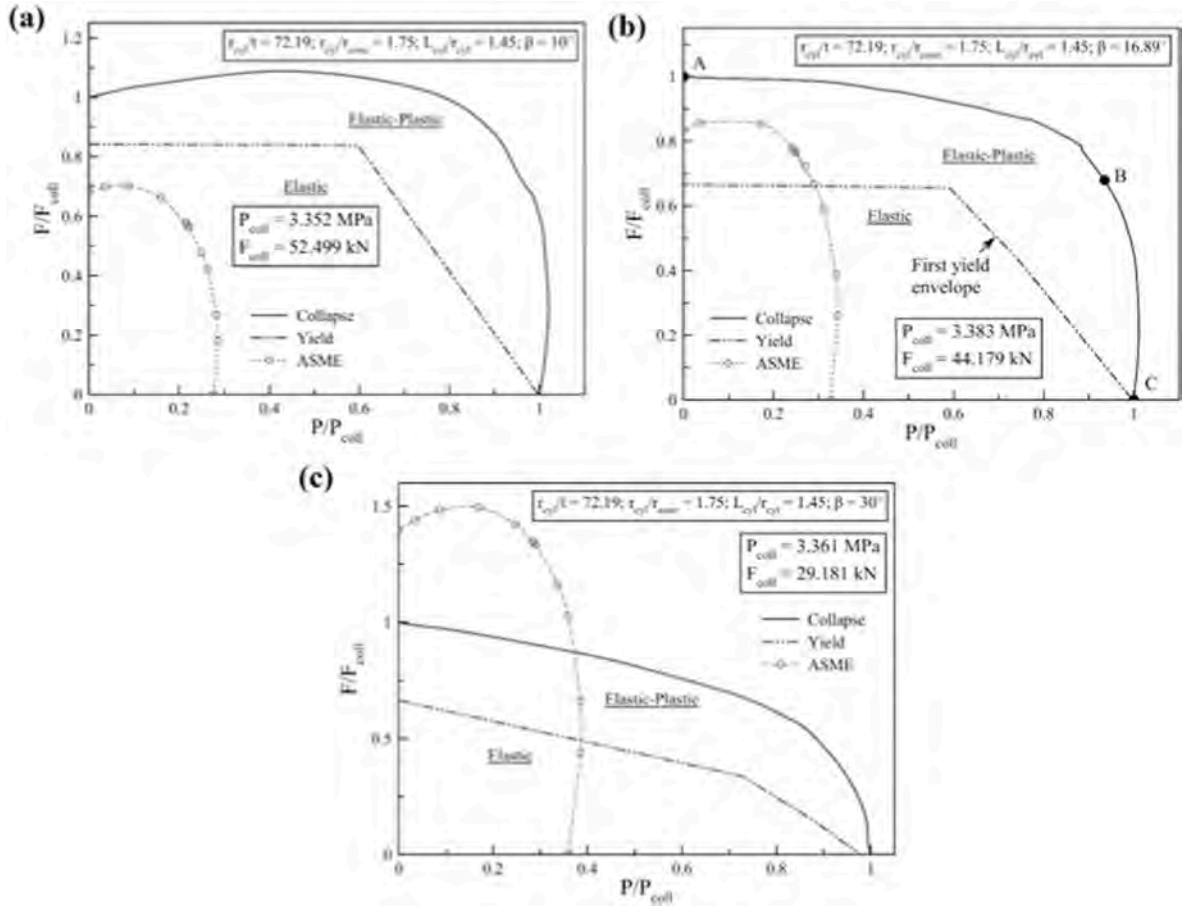

Fig. 14. Combined stability plot for cone-cylinder transition shell in the range of $10° < \beta < 30°$ with constant $r_{cyl}/t = 72.19$ and $r_{cyl}/r_{cone} = 1.75$.

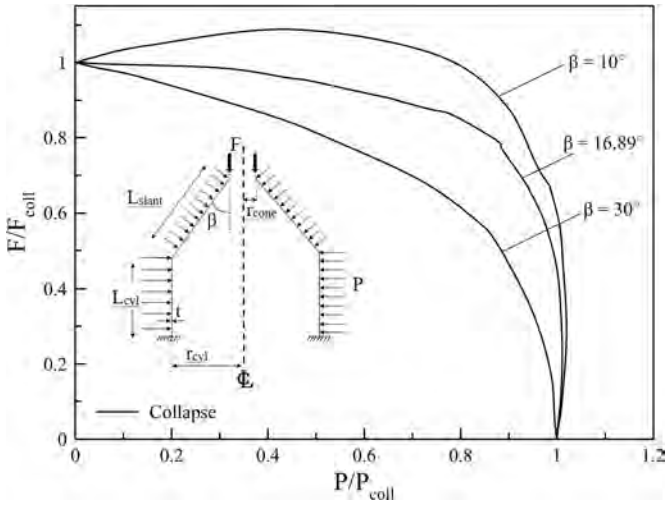

Fig. 15. Domain of combined stability plot for different cone angle, β values.

process generated by the concentrated load. Hühne et al. [43] highlighted that the procedure of the SLI in the finite element analysis has three (3) steps. First, lateral perturbation load, $P_{Perturb}$ is applied at the mid-section of the shell. This is intended to produce a single buckle or a local dent on the shell. At this point, once the required indent/depth is obtained from the lateral perturbation load, $P_{Perturb}$, the load is put on hold thus creating a stress concentration around the vicinity of the shell mid-surface. Then, the shell is driven by external pressure until the buckling load is reached. The interaction between the locally inward dent formed by the magnitude of perturbation load is essential in estimating the load-carrying capacity of the imperfect shell [44]. The amplitude of imperfection calculated using Eurocode 3 [13] guideline, as shown in the following equation (1):

$$L_{gx} = 4\sqrt{r_{cyl}t} \tag{1}$$

Fig. 17 illustrates the location of the applied perturbation load to produce dimple/dent along the cone-cylinder shell length identified as (i) Dent – cone mid-section, (ii) Dent – cone-cylinder intersection and (iii) Dent – cylinder mid-section. This investigation was carried out to examine the cone-cylinder shell imperfection sensitivity as reported in Ref. [39]. Similar boundary conditions employed in the previous section were adopted.

Fig. 18 shows the domain of combined stability plot of the perfect and imperfect cone-cylinder shells at different dimple location. With constant imperfection amplitude of $w_o/t = 0.411$, several cases have been tested for the cone-cylinder shells subjected to a combined load of axial compression and external pressure. The outcome of the result can be outlined as;

i. The imperfect cone-cylinder shell produces a similar domain of combined stability curve in comparison to the perfect shell.
ii. The imperfect cone-cylinder shell is remarkably sensitive at the pressure dominant region compared to the force dominant region
iii. The location of dimple/dent imperfection at cylinder mid-section proves to be the worst-case scenario as it produces a magnitude of the knockdown factor of 0.813. This knockdown factor value demonstrates a drop of nearly 20% of the load-carrying capacity of a perfect shell and being the lowest among the other cases.

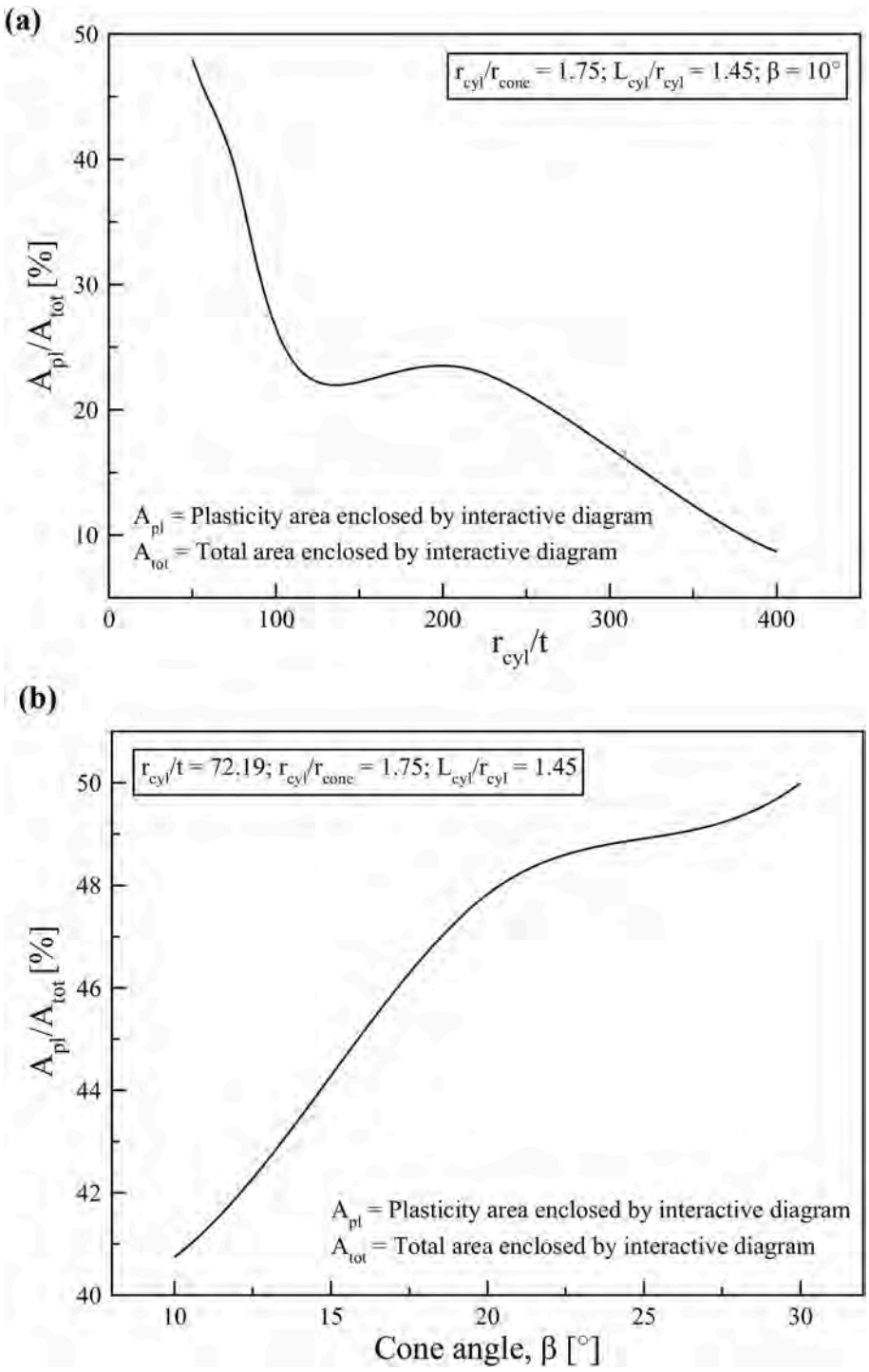

Fig. 16. Plot of the area of plastic strains within the combined stability domain to the total area, against (a) dimensionless-radius-to-thickness ratio and (b) cone angle.

To support the argument above, it is believed that the imperfect cone-cylinder shell (i.e., dent - cylinder mid-section) was further weakened with the presence of external pressure around the shell surface/circumferential area. In contrast, the shell was considerably stronger even with the existence of dimple imperfection at the cone mid-section. This may be linked to the design of the cone angle along with its slant height, as it may slightly resist the applied external pressure.

6. Conclusion

The results of findings following the experimental and numerical investigation of cone-cylinder transition shell subjected to (i) axial compression alone and (ii) combined loading (i.e., axial compression and external pressure) are presented. The reliability of the employed procedure was secured, as the result confirms the repeatability of the experimental data. Besides that, there is a good agreement between experimental and numerical collapse load with discrepancy calculated to be within 10%. Hence, confirming the appropriateness of the

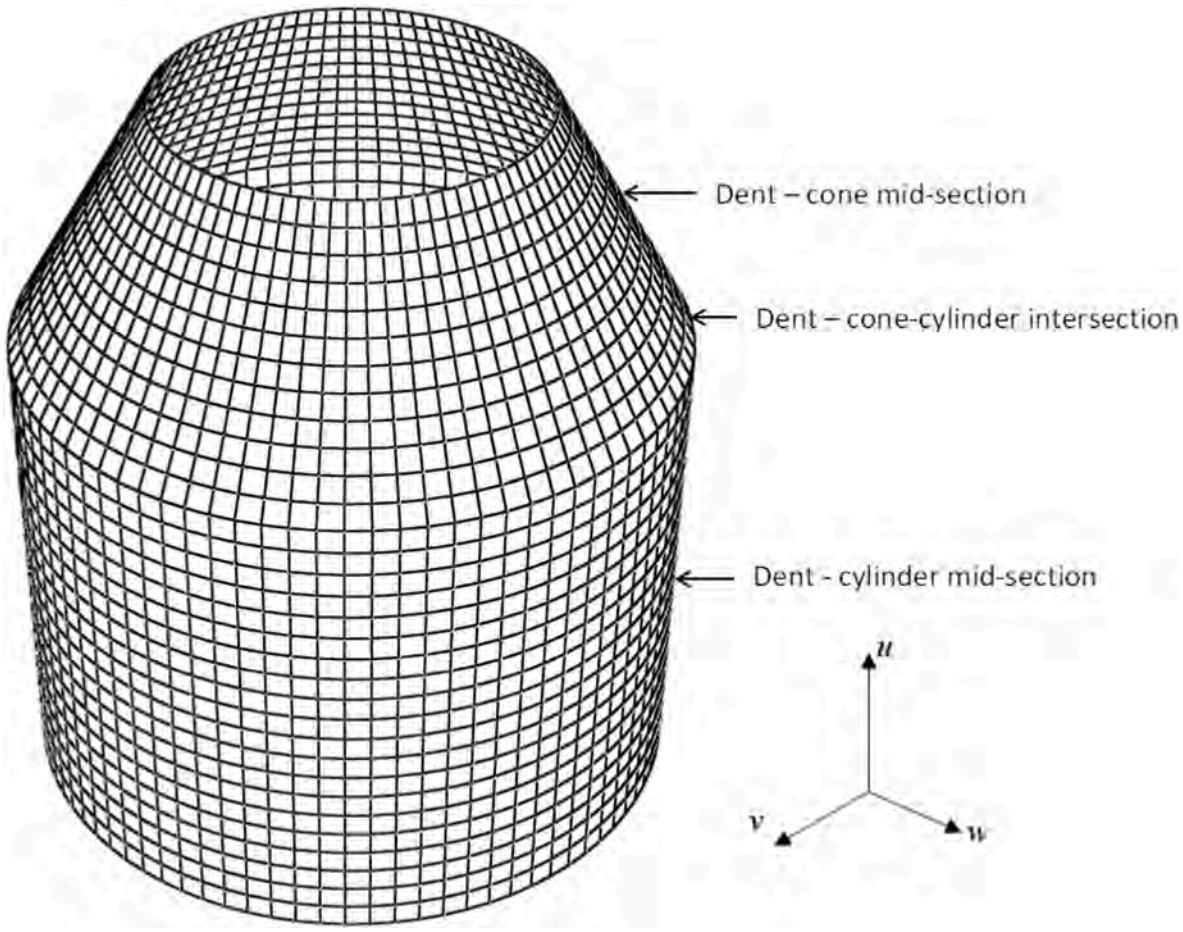

Fig. 17. Location of perturbation load along the cone-cylinder shell length.

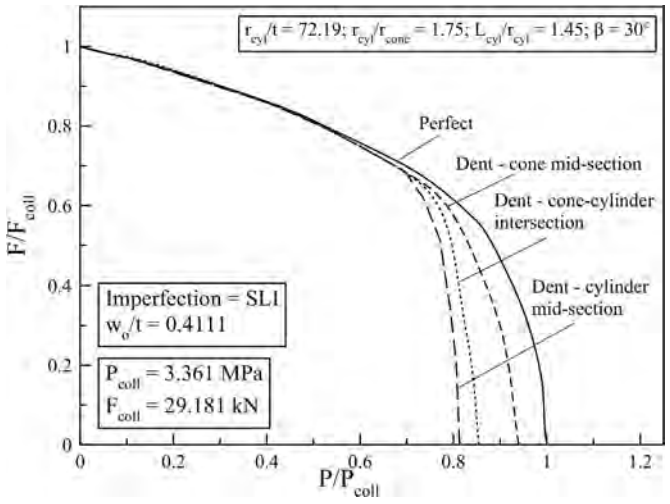

Fig. 18. Domain of combined stability plot of the perfect and imperfect cone-cylinder shells at different dimple location.

numerical approach employed in the study. Numerical analysis of stability domains for cone-cylinder assembly subjected to combined load actions of axial compression and external pressure for a range of geometrical parameters of: (i) $50<r_{cyl}/t<400$ and (ii) $\beta = 10^{\circ}<\beta<30^{\circ}$ were presented. The equivalent cylinder approach was also deployed to complete calculation based on ASME code case 2286-2 for a comparison purpose. From the foregoing analysis, the following conclusions can be drawn: (i) for the case of different dimensionless radius-to-thickness ratio r_{cyl}/t, the result confirms the unsafeness of ASME code case 2286-2 in designing the cone-cylinder shell with $r_{cyl}/t > 400$, (ii) for the case of different cone radius angle, β, it can be said that the ASME code case 2286-2 may perhaps be safe to use in designing the cone-cylinder shell with $\beta < 20^{\circ}$, and constant $r_{cyl}/t = 72.19$ and $r_{cyl}/r_{cone} = 1.75$, (iii) the analysis confirms that increasing the range of (a) dimensionless radius-to-thickness ratio, r_{cyl}/t and (b) increasing the cone radius angle, β, may further shrink the combined stability plot, and, (iv) the cone-cylinder is relatively sensitive to the plastic strain at it wall thickness for the case of different r_{cyl}/t correlated to the changes in cone radius angle, β. In addition, the current design rules may perhaps provide a safe design load against failure, however, subjected to combined loading the situation is relatively unclear and it warrants further investigation. Finally, imperfect cone-cylinder shell under combined loading confirms that (i) the shell is remarkably sensitive at the pressure dominant region compared to the force dominant region and (ii) the location of dimple/dent imperfection at cylinder mid-section proves to be the worst-case scenario.

Author statement

The research data can be shared at the request of the editor.

Declaration of competing interest

The authors declare that they have no known competing financial interests or personal relationships that could have appeared to influence the work reported in this paper.

Acknowledgment

The authors wish to acknowledge the financial assistance received from Universiti Teknikal Malaysia Melaka (UTeM) and the Ministry of Education Malaysia through Fundamental Research Grant Scheme FRGS/2018/FTKMP-CARE/F00386.

References

[1] H. Schmidt, Two decades of research on the stability of steel shell structures at the University of Essen (1985 – 2005): Experiments , evaluations, and impact on design standards, Adv. Struct. Eng. (2018) 1–29, https://doi.org/10.1177/1369433218756273.
[2] A. Zingoni, Discontinuity effects at cone-cone axisymmetric shell junctions, Thin-Walled Struct. 40 (2002) 877–891.
[3] A. Zingoni, B. Mokhothu, N. Enoma, A theoretical formulation for the stress analysis of multi-segmented spherical shells for high-volume liquid containment, Eng. Struct. 87 (2015) 21–31, https://doi.org/10.1016/j.engstruct.2015.01.002.
[4] F.G. Flores, L.A. Godoy, Post-buckling of elastic cone-cylinder and sphere-cylinder complex shells, Int. J. Pres. Ves. Pip. 45 (1991) 237–258, https://doi.org/10.1016/0308-0161(91)90095-J.
[5] J.G. Teng, Elastic buckling of cone-cylinder intersection under localized circumferential compression, Eng. Struct. 18 (1996) 41–48, https://doi.org/10.1016/0141-0296(95)00114-3.
[6] Y. Zhao, J.G. Teng, A stability design proposal for cone-cylinder intersections under internal pressure, Int. J. Pres. Ves. Pip. 80 (2003) 297–309, https://doi.org/10.1016/S0308-0161(03)00048-6.
[7] P. Knoedel, Cylinder-cone-cylinder Intersections under Axial Compression, Buckling of Shell Structures, on Land, in the Sea and in the Air, 1991. London, https://books.google.com.my/books?id=xiweI6w3rI8C&pg=PA296&lpg=PA296&dq=cylinder+cone+cylinder+intersections+under+axial+compression&source=bl&ots=oYbroO2UBr&sig=sw3BZert-Hbg_jUWA7-HGcVdmHg&hl=en&sa=X&ved=0ahUKEwi95ofypdbXAhUTUI8KHal7AoQQ6AEIQjAF#v=onepag. (Accessed 24 November 2017).
[8] H. Schmidt, R. Krysik, Towards Recommendations for Shell Stability Design by Means of Numerically Determined Buckling Loads, Buckling of Shell Structures, on Land, in the Sea and in the Air, London, 1991. https://books.google.com.my/books?id=xiweI6w3rI8C&pg=PA508&dq=Towards+recommendations+for+shell+stability+design+by+means+of+numerically+determined+buckling+loads&hl=en&sa=X&ved=0ahUKEwim2uPYpNbXAhUHq48KHTmKC_sQ6AEIKDAA#v=onepage&q=Towards recommendatio. (Accessed 24 November 2017).
[9] H. Schmidt, Stability of steel shell structures General Report, J. Constr. Steel Res. 55 (2000) 159–181.
[10] H. Schmidt, P. Swadlo, Strength and stability design of unstiffened cylinder/cone/cylinder and cone/cone shell assemblies under axial compression, in: V. Krupka, P. Schneider (Eds.), Proceeding Int. Conf., Brno, Czech Republic, 1997, pp. 361–367. https://www.google.com.my/search?source=hp&ei=9rsXWvuQJcbmvgT_srWQBQ&q=Strength+and+stability+design+of+unstiffened+cylinder%2Fcone%2Fcylinder+and+cone%2Fcone+shell+assemblies+under+axial+compression.+In%3A+Krupka+V%2C+Schneider+P%2C+editors.+Carrying+cap. (Accessed 24 November 2017).
[11] ECCS, ECCS Publication - Buckling of Steel Shells: European Recommendations, 1988.
[12] ECCS, Enhancement of ECCS Design Recommendations and Developement of Eurocode 3 Parts Related to Shells Buckling, Buckling Shells, fifth ed., Brussels Eur. Conv. Constr. Steelwork., 1998, p. 384, https://doi.org/10.1017/CBO9781107415324.004.
[13] ECCS, Buckling of Steel Shells European Design Recommendations, Buckling Shells, fifth ed., Brussels Eur. Conv. Constr. Steelwork., 2008.
[14] J. Błachut, A. Muc, J. Rys, Buckling of unstiffened steel cones subjected to axial compression and external pressure, J. Offshore Mech. Arctic Eng. 135 (2013) 1–9, https://doi.org/10.1115/1.4004953.
[15] R.W. Aylward, G.D. Galletly, D.G. Moffat, Some experimental/theoretical results on the buckling under external pressure of cylinders with various end closures, in: Proc. 2nd Int. SmiRt (Structural Mech. React. Technol. Conf., West Berlin, Germany, 1973, pp. 1–6.
[16] R.W. Aylward, G.D. Galletly, D.G. Moffat, Buckling under external pressure of cylinders with toriconical or pierced torispherical ends: a comparison of experiment with theory, Arch. J. Mech. Eng. Sci. 1–23 (1975) 11–18, https://doi.org/10.1243/JMES_JOUR_1975_017_004_02, 17, 1959-1982.
[17] G.D. Galletly, R.W. Aylward, D. Bushnell, An experimental and theoretical investigation of elastic and elastic-plastic asymmetric buckling of cylinder-cone combinations subjected to uniform external pressure, Ing. Arch. 43 (1974) 345–358, https://doi.org/10.1007/BF00532134.
[18] D. Bushnell, G.D. Galletly, Comparisons of test and theory for nonsymmetric elastic-plastic buckling of shells of revolution, Int. J. Solid Struct. 10 (1974) 1271–1286, https://doi.org/10.1016/0020-7683(74)90072-9.
[19] D. Bushnell, Bifurcation buckling of shells of revolution including large deflections, plasticity and creep, Int. J. Solid Struct. 10 (1974) 1287–1305, https://doi.org/10.1016/0020-7683(74)90073-0.
[20] H. Shen, P. Zhou, T. Chen, Postbuckling analysis of stiffened cylindrical shells under combined external pressure and axial compression, Thin-Walled Struct. 15 (1993) 43–63, https://doi.org/10.1016/0263-8231(93)90012-Y.
[21] H. Shen, T. Chen, Buckling and postbuckling behaviour of cylindrical shells under combined external pressure and axial compression, Thin-Walled Struct. 12 (1991) 321–334, https://doi.org/10.1016/0263-8231(91)90032-E.
[22] O. Ifayefunmi, J. Błachut, Instabilities in imperfect thick cones subjected to axial compression and external pressure, Mar. Struct. 33 (2013) 297–307, https://doi.org/10.1016/j.marstruc.2013.06.004.
[23] O. Ifayefunmi, J. Błachut, The effect of shape, thickness and boundary imperfections on plastic buckling of cones, in: Proc. ASME 2011 30th Int. Conf. Ocean. Offshore Arct. Eng. OMAE2011, 2011, pp. 1–11.
[24] O. Ifayefunmi, Interactive buckling tests on steel cones subjected to axial compression and external pressure – a comparison of experimental data and design codes, Ships Offshore Struct. 9 (2014) 669–679, https://doi.org/10.1080/17445302.2013.862987.
[25] M.K. Chryssanthopoulos, C. Poggi, Collapse strength of unstiffened conical shells under axial compression, J. Constr. Steel Res. 57 (2001) 165–184.
[26] T. Weller, J. Singer, Experimental studies on buckling of ring-stiffened conical shells under axial compression applicability of the linear theory, Exp. Mech. 10 (1970) 449–457.
[27] A. Spagnoli, M.K. Chryssanthopoulos, Elastic buckling and postbuckling behaviour of widely-stiffened conical shells under axial compression, Eng. Struct. 21 (1999) 845–855, https://doi.org/10.1016/S0141-0296(98)00036-4.
[28] A. Spagnoli, Buckling Behaviour and Design of Stiffened Conical Shells under Axial Compression, Unpublished Phd Thesis, University of London, London, 1997.
[29] A. Spagnoli, Different buckling modes in axially stiffened conical shells, Eng. Struct. 23 (2001) 957–965, https://doi.org/10.1016/S0141-0296(00)00112-7.
[30] J. Singer, A. Berkovits, T. Weller, O. Ishai, M. Baruch, O. Harari, Experimental and theoretical studies on buckling of conical and cylindrical shells under combined loading, TA Rep. 48 (1966) 69–84.
[31] J. Arbocz, C.D. Babcock Jr., J. Singer, Buckling of imperfect stiffened cylindrical shells under axial compression, AIAA J. 9 (1971) 68–75, https://doi.org/10.2514/3.6125.
[32] T. Weller, J. Singer, Experimental studies on buckling of 7075-T6 Aluminium alloy integrally stringer-stiffened shells, TA Rep. (1971).
[33] T. Weller, J. Singer, Further experimental studies on buckling of integrally ring-stiffened cylindrical shells under axial compression, Exp. Mech. (1974) 267–273.
[34] J. Singer, A. Rosen, The influence of boundary conditions on the buckling of stiffened cylindrical shells, in: Buckling Struct, Springer-Verlag, Cambridge, United State of America, 1976, https://doi.org/10.1007/978-3-642-50992-6.
[35] BS EN 10002-1, Tensile Testing of Metallic Materials, Part (1), Method of Test at Ambient Temperature, British Standard Institute, London, UK, 2001. https://shop.bsigroup.com/ProductDetail/?pid=000000000019970662. (Accessed 11 September 2018).
[36] O. Ifayefunmi, Buckling behavior of axially compressed cylindrical shells: comparison of theoretical and experimental data, Thin-Walled Struct. 98 (2016) 558–564, https://doi.org/10.1016/j.tws.2015.10.027.
[37] J. Błachut, O. Ifayefunmi, M. Corfa, Collapse and buckling of conical shells, Proc. Int. Offshore Polar Eng. Conf. (2011) 887–893.
[38] American Society of Mechanical Engineers (ASME), Code Case 2286-2, Alternative Rules for Determining Allowable External Pressure and Compressive Stresses for Cylinders, Cones, Sphere and Formed Heads, Section VII, Divisions 1 and 2. Cases of the ASME Boiler and Pressure Vessel Code, America, New York, 2008. http://standards.globalspec.com/std/1594065/asme-bpvc-n-284. (Accessed 21 February 2017).
[39] M.S. Ismail, O. Ifayefunmi, S.H.S.M. Fadzullah, Buckling of imperfect cylinder-cone-cylinder transition under axial compression, Thin-Walled Struct. 144 (2019) 106250, https://doi.org/10.1016/j.tws.2019.106250.
[40] M.S. Ismail, O. Ifayefunmi, S.H.S.M. Fadzullah, The role of stiffener in resisting buckling of externally pressurized cone-cylinder intersection the role of stiffener in resisting buckling of externally pressurized cone - cylinder intersection, in: Proc. Mech. Eng. Res. Day, 2018, pp. 55–56.
[41] J. Błachut, Load bearing of corroded shells under external/internal pressure, J. Struct. Integr. Maint. 3 (2018) 217–226, https://doi.org/10.1080/24705314.2018.1535752.
[42] J. Błachut, Buckling of corroded torispherical shells under external pressure, Am. Soc. Mech. Eng. Press. Vessel. Pip. Div. PVP 3B (2018) 1–7, https://doi.org/10.1115/PVP2018-84309.
[43] C. Hühne, R. Rolfes, E. Breitbach, J. Teßmer, Robust design of composite cylindrical shells under axial compression — simulation and validation, Thin-Walled Struct. 46 (2008) 947–962. http://linkinghub.elsevier.com/retrieve/pii/S0263823108000438. (Accessed 7 July 2014).
[44] M.A. Arbelo, R. Zimmermann, S.G.P. Castro, Comparison of new design guidelines for composite, in: Ninth Int. Conf. Compos. Sci. Technol., Sorrento, Italy, 2013, pp. 96–111.